Available online at www.sciencedirect.com
ScienceDirect
Energy Procedia 1 (2009) 2177–2184
Energy Procedia
www.elsevier.com/locate/procedia

GHGT-9

# Detection of surface deformation related with $CO_2$ injection by DInSAR at In Salah, Algeria

Takumi Onuma[a]* and Shiro Ohkawa[b]

[a]JGI, Inc.,1-5-21, Otsuka, Bunkyo-ku, Tokyo 112-0012, Japan
[b]Japan Petroleum exploration Co., Ltd., 1-7-12, Marunouchi, Chiyoda-ku, Tokyo 100-0005, Japan

**Abstract**

Surface deformation around $CO_2$ injection wells at In Salah, Algeria was analyzed by satellite-borne SAR data. The surface heave rate up to 7 mm/year was detected around all of the three injection wells. The analysis of the deformation series has revealed that each injection well has different deformation history. The surface heave pattern shows a NW-SE trending elongation which is the direction of the anticline axis, suggesting certain relationship between the structural feature and the distribution of injected $CO_2$. This technique will hopefully provide us with a powerful and a cost-effective tool for monitoring of behaviors of the injected $CO_2$.



*Keywords:* Differential Interferometry SAR; $CO_2$ injection; Surface deformation monitoring; In Salah; Stacking

## 1. Introduction

InSAR, standing for Interferometric Synthetic Aperture Radar, has been proved as a promising remote sensing technique for mapping of topography and monitoring of ground displacement at an order of centimeters or millimeters. Several spaceborne SAR systems including ALOS PALSAR, JERS-1 SAR, ERS1/2 AMI, ENVISAT ASAR and Radarsat SAR, have been widely used for mapping of surface deformation. These are referred to as the active type sensors which transmit radar pulses towards the earth and receive echoes back off the Earth's surface. Because of the nature of radio wave, spaceborne SAR systems have the observation capability at all weather, day and night conditions, which is suitable for monitoring of Earth's surface. Although many InSAR application examples related with earthquakes, volcanic activity, landslide, glaciers motion, and ground subsidence have been reported in the past decade [1][2], to date there is no examples concerning with the monitoring of $CO_2$ injection. The primary objective of this paper is to investigate the applicability of satellite-borne InSAR technique to the monitoring of surface deformation at $CO_2$ injection site, by applying the technique on the actual project being operated at In Salah, Algeria (Figure 1).

* Corresponding author. Tel.: +81-3-5978-8052; fax: +81-3-5978-8058.
*E-mail address*: onuma@jgi.co.jp.

doi:10.1016/j.egypro.2009.01.283

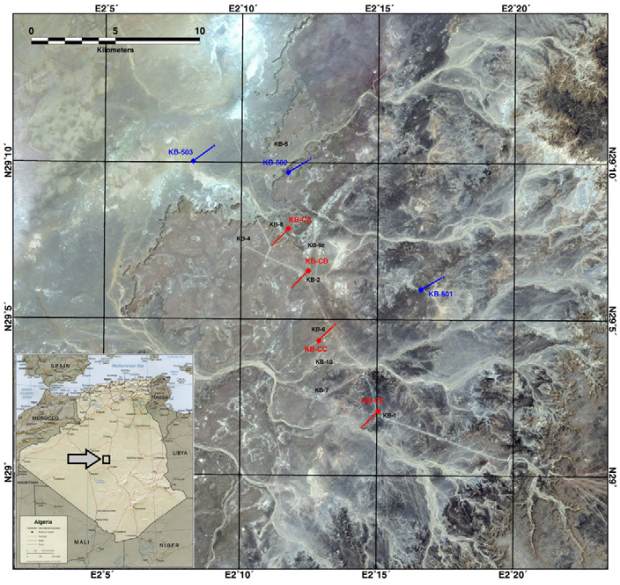


Figure 1. Landsat7 ETM+ image of the In Salah Gas Project with $CO_2$ injection wells (blue lines) and gas production wells (red lines). Well locations after [4].

In Salah Gas Project is well known as one of huge CCS (Carbon dioxide Capture and Storage) projects in the world, as well as the Sleipner Project, Norway and Weyburn Project, Canada. The $CO_2$ is separated from natural gas produced from three fields of Krechba, Reg, and Teguentour, and is injected into underground at three wells down-dip from the Krechba natural gas accumulation. The field is located in the rocky desert where ground surface is vegetation free. In such a dry area, radar signal scattered at surface objects is generally quite coherent for different observations, which is suitable for the InSAR processing. Natural gas produced in the project contains 3-9% of carbon dioxide which is captured by a regenerative amine system [3] then is injected into the Carboniferous reservoir at a depth of 1,900m, from three injection wells of KB-501, 502 and 503 [4]. Monitoring at In Salah Gas Project is considered to be crucial for developing a detailed understanding of behaviors of injected $CO_2$ with reducing uncertainties in predictions of long term storage performance [5]. Monitoring methods can be separated into seismic and non-seismic techniques; seismic techniques include microseismic and 4D seismic surveys and non-seismic techniques may comprise of borehole gravity, resistivity changes, and controlled source electromagnetics (CSEM) [3]. A large number of observations are required for all of these geophysical methods and generally the data acquisition may be performed at great expense. Although InSAR technique cannot sense injected $CO_2$ directly, the coverage of such broad area as 100km x 100km by one satellite SAR scene and repeated observations, for instance every 35 days in case of ENVISAT ASAR, make InSAR as a cost-effective method for monitoring. Adding to these advantages, because the history of surface deformation can be one of supplemental data to refine the model of underground distribution of injected $CO_2$, the InSAR results is expected to contribute to numerical modeling when combined with results of traditional geophysical surveys.

## 2. Methodology

SAR data is a complex image that retains amplitude and phase. InSAR technique exploits the phase difference between two observations, which can be converted to the distance along the line of radar illumination, referred to as the Line of Sight (LOS), and to the height using SAR look angle and platform altitude. Detailed explanation and discussion on the basic of InSAR technique is out of the scope of this paper, and is introduced in [1]; the extension of InSAR technique, Differential InSAR (DInSAR), and the stacking of the differential phase are the keys for the work of this paper.

In DInSAR technique, the phase difference corresponding to the deformation occurred between two acquisitions is derived by subtracting the topographic phase component of the master SAR image (usually older acquisition of a pair) from the initial interferogram. Topographic phase is simulated from the digital elevation model (DEM) and the baseline, the distance between two sensors that is calculated from the orbit data. The difference is referred to as the differential interferogram. The phase of the differential interferogram $\delta\phi$ is expressed as

$$\delta\phi \approx \frac{4\pi}{\lambda}\left[d_2 - d_1\right] + \Delta\phi_{atm} + \Delta\phi_{base} + \Delta\phi_{topo} + \Delta n \qquad (1)$$

where $\lambda$ is the wavelength of the SAR system, $d_1$ and $d_2$ are LOS projections of the cumulative deformations, $\Delta\phi_{atm}$ is the tropospheric turbulence phase [6], $\Delta\phi_{base}$ is the phase resulted from the baseline estimation error, $\Delta\phi_{topo}$ is the topographic artifacts which may be contained in DEM and $\Delta n$ accounts for the phase noise due to the decorrelation phenomena. The first term of righthand side of Eq. (1) is the deformation phase component which is the target of the DInSAR analysis. Therefore, other four terms should be eliminated from the differential interferogram. Apart from the displacement caused by earthquakes or landslides, the subsidence due to pumping up of groundwater and the displacement attributed to crustal deformation are long lasting phenomena that can be considered as temporally coherent, whereas tropospheric turbulence and phase noise are coherent in space but not in time domain. Taking this character of "phase noise" into account, when a number of interferograms are available, the influence of $\Delta\phi_{atm}$ and $\Delta n$ on the differential phase can be reduced with emphasizing temporally coherent signal such as subsidence or upheaval by stacking of differential phase. It is the phase rate which is derived from the stacking, and further refinement of differential phase (e.g. reduction of phase noise) is feasible by using the phase rate as a starting model of the deformation. Obviously, selection of interferograms with long interval and with short baseline leads to better result. Because the longer the interval, the larger the cumulative amount of displacement, which makes the ratio of phase noise to the differential phase small. Stacking is performed by weighted sum of individual differential phases with the time interval of the interferogram as a weight [7]. The stacking of multiple interferograms is the simplest but robust approach comparing with other advanced ones such as Point Target analysis [8] and Small Baseline Subset Algorithm [9]. Although the precise orbit state vectors for an interferometry pair can be used for the calculation of the baseline, the one calculated from the orbit information may contain certain error that is one of sources of phase error in the differential interferogram. This can be reduced by the refined baseline calculated from the height data of ground control points (GCP) extracted from DEM and corresponding differential phase. DEM data used in the work is the Shuttle Radar Topography Mission version 2 of 3-arcsecond (SRTM3), of which cell size is about 90m x 90m. The area of the In Salah Gas Project is characterized by the distribution of low relief hills with elevation ranging from 420m to 580m. Considering this topographic feature of the area as well as the accuracy of the SRTM3 and the interferogram pixel dimension of 80m x 90m, the contribution of $\Delta\phi_{topo}$ in Eq. (1) to the differential phase is negligible.

## 3. Results

Interferogram generation and stacking was performed using 30 scenes of ENVISAT ASAR data spanning from July 2003 to May 2008, on descending orbits (track 65; see Table 1). ENVISAT ASAR is the C band radar system with the wavelength of 5.6cm and the revisit cycle of 35 days. In total 129 interferometry pairs meet with the requirement of the perpendicular baseline less than 300m. Interferograms were produced for all pairs with 4 looks in range direction and 20 looks in azimuth direction, resulting in the ground pixel size of 80m x 90m. Multilooking process with such large number of looks can reduce the phase noise and improve the coherence of an interferogram. Baseline refinement was performed using elevation of GCPs extracted from the area with coherence value higher than 0.5. Among them, 115 pairs have the slave scene (later acquisition of a pair) acquired after August 2004, when the $CO_2$ injection has started. Finally 56 pairs (Table 2) without severe tropospheric turbulence patterns and with the observation interval longer than 1.5 years are adopted for stacking differential phase, in order to obtain the surface deformation rate with minimizing the influence of tropospheric turbulence and phase noise. Detected deformation rate map is shown in Figure 2. The result of stacking shows that surface upheaval rate up to 7 mm/year was detected around all of the three injection wells, whereas a subsidence rate of 4 mm/year for the gas-producing wells. Considering the agreement of locations of three injection wells and upheaval patterns, it is obvious that DInSAR stacking process using satellite-borne SAR data has successfully detected the surface deformations associated with $CO_2$ injection. All of the surface heave for injectors and the subsidence for producers show a NW-SE trending

Table 1. ENVISAT ASAR Data used.
Bp: Perpendicular baseline of the interferogram with the scene of 2004/7/31 as the master data.

| Orbit | Year | Month | Day | Bp (m) | Days from 2004/7/31 |
|---|---|---|---|---|---|
| 7133 | 2003 | 7 | 12 | -1052 | -385 |
| 7634 | 2003 | 8 | 16 | -1029 | -350 |
| 8636 | 2003 | 10 | 25 | 338 | -280 |
| 9137 | 2003 | 11 | 29 | -116 | -245 |
| 9638 | 2004 | 1 | 3 | 445 | -210 |
| 10640 | 2004 | 3 | 13 | 442 | -140 |
| 11141 | 2004 | 4 | 17 | 132 | -105 |
| 11642 | 2004 | 5 | 22 | 154 | -70 |
| 12143 | 2004 | 6 | 26 | -687 | -35 |
| 12644 | 2004 | 7 | 31 | 0 | 0 |
| 13145 | 2004 | 9 | 4 | 563 | 35 |
| 13646 | 2004 | 10 | 9 | 213 | 70 |
| 14147 | 2004 | 11 | 13 | -942 | 105 |
| 14648 | 2004 | 12 | 18 | -467 | 140 |
| 15149 | 2005 | 1 | 22 | -316 | 175 |
| 15650 | 2005 | 2 | 26 | -390 | 210 |
| 17153 | 2005 | 6 | 11 | -457 | 315 |
| 18656 | 2005 | 9 | 24 | -48 | 420 |
| 20660 | 2006 | 2 | 11 | -746 | 560 |
| 21161 | 2006 | 3 | 18 | -29 | 595 |
| 22664 | 2006 | 7 | 1 | 628 | 700 |
| 23165 | 2006 | 8 | 5 | 838 | 735 |
| 25169 | 2006 | 12 | 23 | 58 | 875 |
| 26171 | 2007 | 3 | 3 | 52 | 945 |
| 30179 | 2007 | 12 | 8 | -682 | 1225 |
| 30680 | 2008 | 1 | 12 | -305 | 1260 |
| 31181 | 2008 | 2 | 16 | -610 | 1295 |
| 31682 | 2008 | 3 | 22 | -92 | 1330 |
| 32183 | 2008 | 4 | 26 | -413 | 1365 |
| 32684 | 2008 | 5 | 31 | -279 | 1400 |

Table 2. Interferometry pairs used for stacking operation. Pairs with |Bp| less than 300m were chosen.

| No. | Master | Slave | Bp(m) | Days | No. | Master | Slave | Bp(m) | Days |
|---|---|---|---|---|---|---|---|---|---|
| 1 | 2003/8/16 | 2006/2/11 | 283 | 560 | 29 | 2004/10/9 | 2006/3/18 | -242 | 525 |
| 2 | 2003/10/25 | 2006/7/1 | 290 | 700 | 30 | 2004/10/9 | 2006/12/23 | -154 | 805 |
| 3 | 2003/10/25 | 2006/12/23 | -280 | 875 | 31 | 2004/10/9 | 2007/3/3 | -161 | 875 |
| 4 | 2003/10/25 | 2007/3/3 | -286 | 945 | 32 | 2004/11/13 | 2007/12/8 | 260 | 1120 |
| 5 | 2003/11/29 | 2006/3/18 | 87 | 595 | 33 | 2004/12/18 | 2007/12/8 | -214 | 1085 |
| 6 | 2003/11/29 | 2006/12/23 | 175 | 875 | 34 | 2004/12/18 | 2008/1/12 | 162 | 1120 |
| 7 | 2003/11/29 | 2007/3/3 | 168 | 945 | 35 | 2004/12/18 | 2008/2/16 | -143 | 1155 |
| 8 | 2003/11/29 | 2008/1/12 | -189 | 1260 | 36 | 2004/12/18 | 2008/4/26 | 55 | 1225 |
| 9 | 2003/11/29 | 2008/3/22 | 24 | 1330 | 37 | 2004/12/18 | 2008/5/31 | 188 | 1260 |
| 10 | 2003/11/29 | 2008/4/26 | -296 | 1365 | 38 | 2005/1/22 | 2008/1/12 | 11 | 1085 |
| 11 | 2003/11/29 | 2008/5/31 | -163 | 1400 | 39 | 2005/1/22 | 2008/2/16 | -294 | 1120 |
| 12 | 2004/1/3 | 2006/7/1 | 183 | 700 | 40 | 2005/1/22 | 2008/3/22 | 224 | 1155 |
| 13 | 2004/3/13 | 2006/7/1 | 186 | 700 | 41 | 2005/1/22 | 2008/4/26 | -96 | 1190 |
| 14 | 2004/4/17 | 2006/3/18 | -161 | 595 | 42 | 2005/1/22 | 2008/5/31 | 37 | 1225 |
| 15 | 2004/4/17 | 2006/12/23 | -74 | 875 | 43 | 2005/2/26 | 2007/12/8 | -292 | 1015 |
| 16 | 2004/4/17 | 2007/3/3 | -80 | 945 | 44 | 2005/2/26 | 2008/1/12 | 85 | 1050 |
| 17 | 2004/4/17 | 2008/3/22 | -224 | 1330 | 45 | 2005/2/26 | 2008/2/16 | -220 | 1085 |
| 18 | 2004/6/26 | 2006/2/11 | -59 | 560 | 46 | 2005/2/26 | 2008/3/22 | 298 | 1120 |
| 19 | 2004/6/26 | 2007/12/8 | 5 | 1225 | 47 | 2005/2/26 | 2008/4/26 | -23 | 1155 |
| 20 | 2004/6/26 | 2008/2/16 | 77 | 1295 | 48 | 2005/2/26 | 2008/5/31 | 111 | 1190 |
| 21 | 2004/6/26 | 2008/4/26 | 274 | 1365 | 49 | 2005/9/24 | 2008/1/12 | -257 | 840 |
| 22 | 2004/7/31 | 2006/3/18 | -29 | 595 | 50 | 2005/9/24 | 2008/3/22 | -44 | 910 |
| 23 | 2004/7/31 | 2006/12/23 | 58 | 875 | 51 | 2005/9/24 | 2008/5/31 | -231 | 980 |
| 24 | 2004/7/31 | 2007/3/3 | 52 | 945 | 52 | 2006/2/11 | 2007/12/8 | 64 | 665 |
| 25 | 2004/7/31 | 2008/3/22 | -92 | 1330 | 53 | 2006/2/11 | 2008/2/16 | 136 | 735 |
| 26 | 2004/7/31 | 2008/5/31 | -279 | 1400 | 54 | 2006/3/18 | 2008/1/12 | -276 | 665 |
| 27 | 2004/9/4 | 2006/7/1 | 65 | 665 | 55 | 2006/3/18 | 2008/3/22 | -63 | 735 |
| 28 | 2004/9/4 | 2006/8/5 | 275 | 700 | 56 | 2006/3/18 | 2008/5/31 | -250 | 805 |

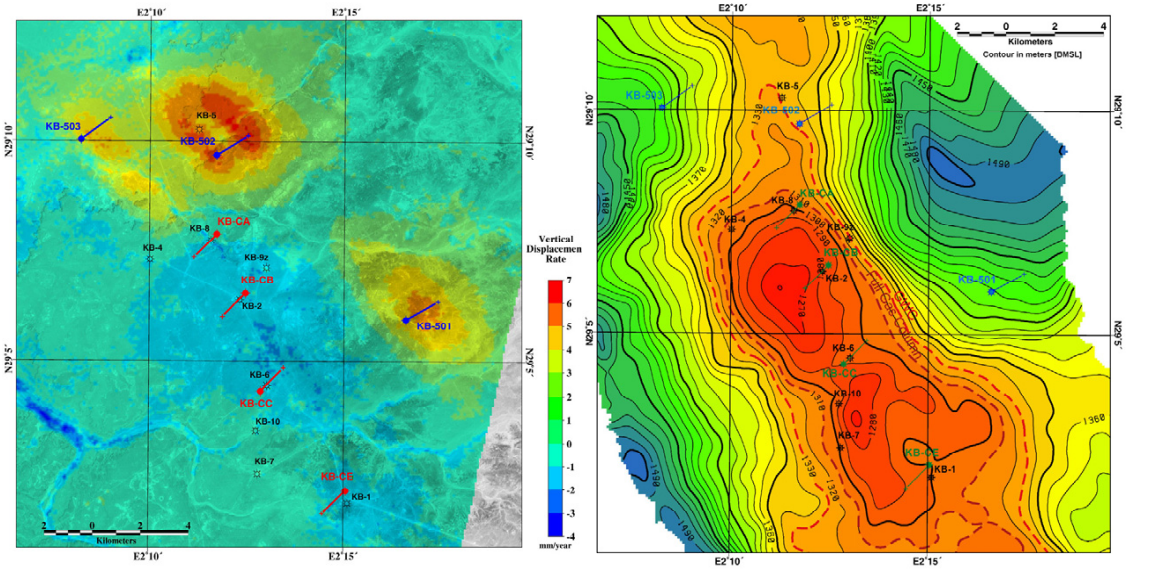


Figure 2. (a) Vertical displacement rate of the term from 2004/7/31 to 2008/5/31 around the Krechba field detected by DInSAR stacking, using 56 differential interferograms. Background: Landsat7 ETM+ PAN B/W image. (b) Top reservoir structure map adopted from [4]. KB-501, 502 and 503 are $CO_2$ injection wells and KB-CA, CB, CC, CD are gas-producers. Note the agreement between upheaval patterns and $CO_2$ injection wells in (a). All of surface heave for injectors and subsidence for producers show a NW-SE trending elongation pattern which is concordant with structural feature as shown in (b).

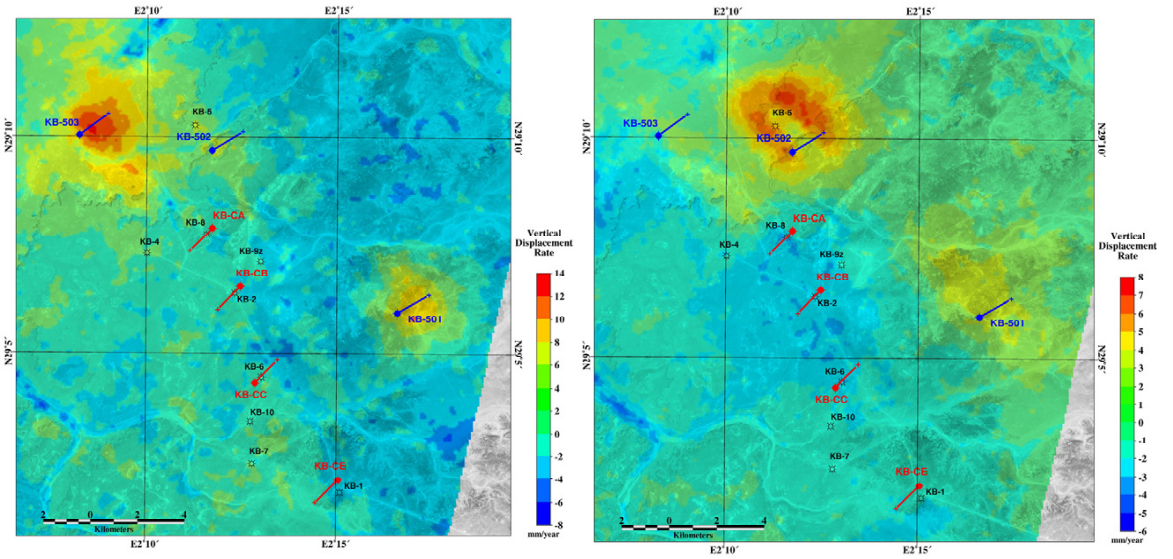


Figure 3. Vertical displacement rates detected by DInSAR stacking of terms (a) from 2004/7/31 to 2005/9/24, and (b) from 2005/9/24 to 2008/5/31. Note the upheaval rate changes around KB-502 and KB-503 before and after 2005/9/24.

elongation pattern which is the direction of the anticline axis of the field, suggesting certain relationship between the structural feature and the distribution of injected $CO_2$.

In order to investigate the deformation history, all of 129 interferograms were visually re-inspected, and it was found that the upheaval pattern around the injection well of KB-502 was hardly identified at the early stage of the injection, until Sept. 24, 2005. This is clearly confirmed by maps showing vertical displacement rate for terms from Jul. 31, 2004 to Sept. 24, 2005 and from Sept. 24, 2005 to May 31, 2008, which are detected by separate stacking processes. The upheaval rate around KB-502 before Sept. 24, 2005 is very small as shown in Figure 3 (a), whilst it reaches 8mm/year after the date shown as in (b). In contrast, the upheaval rate around KB-503 before Sept. 24, 2005 is as high as 14mm/year, but it decreases down to 2-4mm/year in later stage.

The sum of the displacement calculated from interferometry pairs, whose intervals are successive from the start of the $CO_2$ injection, can be treated as the displacement for a single interval. This is a chain of the interferograms, such that the slave of an interferogram is the master of the succession. For each date of the slave scene of interferometry pairs, the vertical displacement since Jul. 31, 2004 was calculated, by averaging displacement values calculated from interferometry pairs of single interval and of successive intervals. This slave-date based sequence of vertical displacement results in formulating the deformation time series from the start of $CO_2$ injection. Resulted deformation time series for selected 12 dates are shown in Figure 4. It seems that areas around KB-501 and KB-503 start swelling up soon after the commencement of $CO_2$ injection, and surface heave around KB-502 appears to start about Sept. 2005. Upheaval rate around KB-503 after August, 2006 seems to decrease, whereas the rate around KB-502 increases. In order to understand the deformation history around three injection wells and producers, four small areas shown in the last map of the series in Figure 4 were selected, and displacement values for these areas were averaged. Detected deformation histories for these areas are shown in Figure 5. It is clearly demonstrated that KB-501 and KB-503 start to swell up soon after the injection of $CO_2$ with very high rate of +14mm/year at KB-503, and upheaval rate for KB-502 increases at around 800 days (since Jul. 12, 2003), which corresponds to Sept. 24, 2005 in our dataset. Upheaval pattern around KB-501 is an intermediate type of KB-502 and KB-503. Subsidence rate around producers is very small but it appears to be constant.

As well demonstrated in Figures 2 (a) and 3 (b), the displacement rate around KB-502 is peculiar and shows a horseshoe-like pattern. To investigate the deformation history around KB-502 in detail, many small areas with 5 pixels * 5 pixels (of multi-looked image) in size were arranged so that the relationship between the deformation

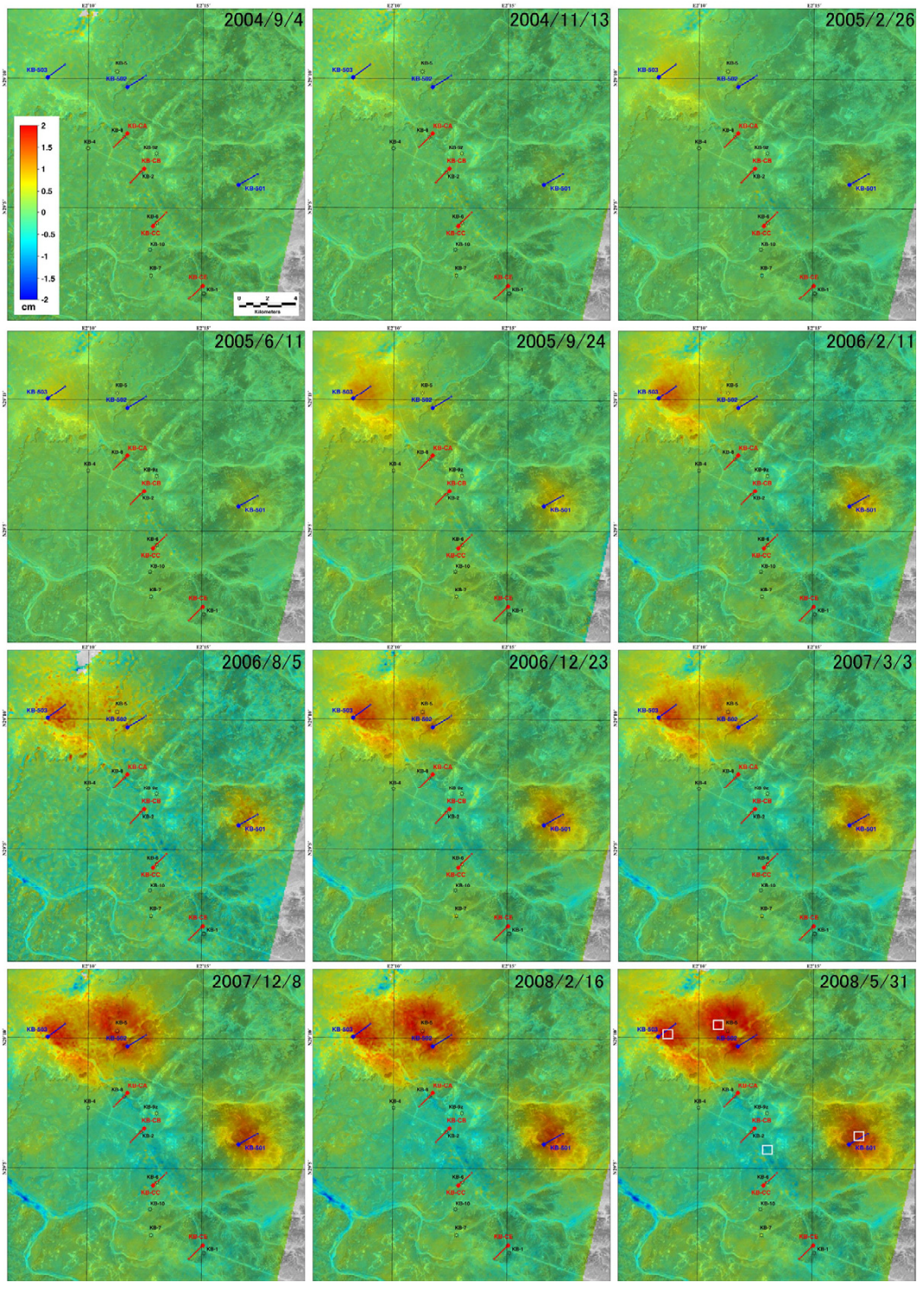


Figure 4. Deformation time series with respect to July 31, 2004 for selected 12 dates. Areas around KB-501 and KB-503 started swelling soon after the commencement of $CO_2$ injection. Upheaval around KB-502 appears to start about September 2005.

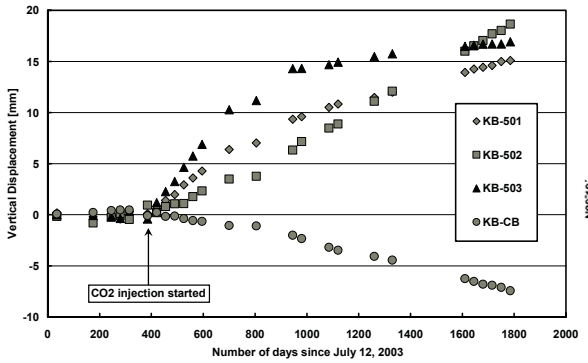


Figure 5. Deformation history measured for areas around three injection wells of KB-501 - 503 and a gas producing well of KB-CB. Locations of areas are marked as white squares in the deformation map of 2008/5/31 in Figure 4. Note three injection wells have different deformation history.

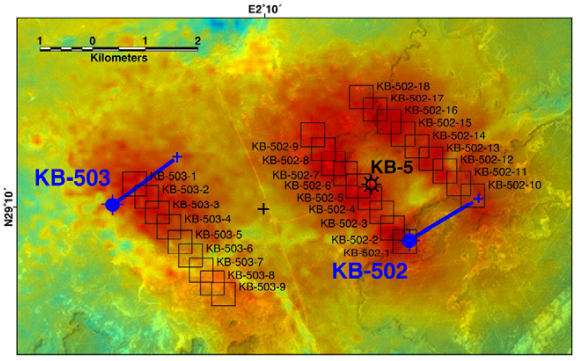


Figure 6. Vertical displacement around $CO_2$ injection wells of KB-502 and KB-503 for the interval between Jul. 31, 2004 and May 31, 2008 with localities of measurements for the deformation time series. Well marks for KB-502 and 503 locate the well head.

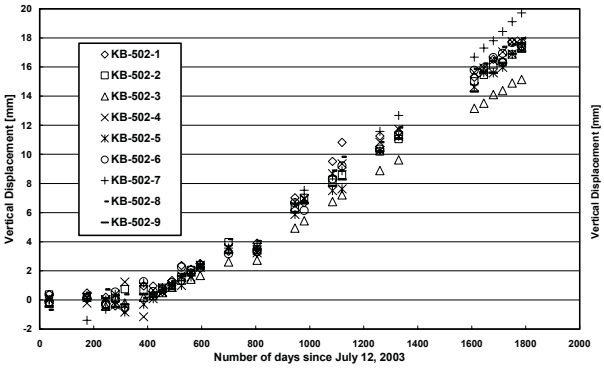


Figure 7. Deformation time series measured for areas of KB-502-1 through KB-502-9 around the injection well of KB-502. Note swelling starts soon after the commencement of $CO_2$ injection in all areas, regardless of the distance from the well. Localities are shown in Figure 6.

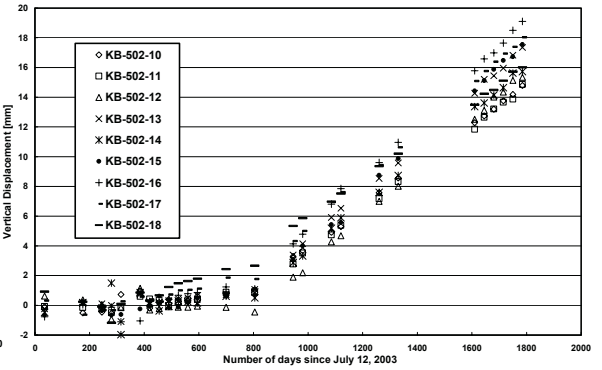


Figure 8. Deformation time series measured for areas of KB-502-10 through KB-502-18 around the injection well of KB-502. Note in most area swelling seems to start about 200 – 400 days after the commencement of $CO_2$ injection (600 – 800 days since July 12, 2003), suggesting certain relationship between the delay and the distance from the well head. Localities are shown in Figure 6.

history and the distance from the injection well can be examined (Figure 6). Location of the well head of KB-502 is marked by a well symbol in Figure 6, and $CO_2$ is injected from SW to NE along a horizontal well. Deformation history of a sequence of KB-502-1 through KB-502-9 is shown in Figure 7, which suggests that all small areas begin to swell immediately after the starting of $CO_2$ injection and almost simultaneously, regardless to the distance from the well. This may imply that $CO_2$ can migrate with very high velocity at the beginning of injection (note KB-502-9 is about 3km away from the well head). The same deformation pattern was confirmed for a sequence of KB-503-1 through KB-503-9. In contrast, the deformation history of a sequence of KB-502-10 through KB-502-18 shown in Figure 8 indicates that the upheaval around the tail of the well does not start immediately after the injection, and KB-502-10 through KB-502-16 begin to swell up about 200-400 days after the starting of injection.

Because no information on the operation of the injection is available, the discussion on the relationship between the delay of upheaval and the distance from the well is not feasible. Also, the evaluation of the accuracy on the results of the analysis could not be covered in this paper, simply due to lack of reference data for verification such as the injection history or leveling survey data. However, judging from the agreement between displacement patterns and locations of injectors and producers, there is no doubt that the DInSAR analysis has successfully revealed the surface deformation related with $CO_2$ injection.

## 4. Conclusion

Surface deformation pattern related with $CO_2$ injection at In Salah Gas Project, Algeria, was successfully analyzed by DInSAR using 30 ENVISAT ASAR data spanning from Jul. 2003 to May 2008. Vertical deformation rates were derived by the stacking of differential phases and the quality of differential phase was greatly improved using phase rates derived from stacking techniques. Deformation time series was constructed using chronological chains of interferograms and it was found from the deformation series that each injection well experienced different deformation history. Results of DInSAR analysis indicates that surface around KB-501 and KB-503 starts swelling up immediately after the commencement of $CO_2$ injection with very high rate of +14mm/year at KB-503 and +8mm/year at KB-501, whereas upheaval of KB-502 seems to start about Sept. 2005. Detailed measurement using deformation time series has revealed that even at KB-502 the upheaval starts immediately after the $CO_2$ injection in southern part, and around the tail of the horizontal well in northern part it begins about Sept. 2005. Upheaval rate at KB-503 decreases around Sept. 2005 and at KB-501 as well. Subsidence rate of -3mm/year was detected around the producers and it appears to be constant. Although the verification of the results was not performed simply due to lack of reference data, judging from the agreement between deformation patterns and well locations it is obvious that the DInSAR analysis using satellite-borne SAR data is promising technique for monitoring of surface deformation related with $CO_2$ injection in the area. All weather, day and night observation capability of satellite-borne SAR systems and the huge archive of repeated observations provide us with cost-effective monitoring tool comparing with other conventional geophysical surveys. When adequate number of interferometry pairs are available, the deformation time series can be detected, which may be one of supplemental data to refine the model of underground distribution of injected $CO_2$. Accordingly, the DInSAR result is expected to contribute to numerical modeling when combined with results of traditional geophysical surveys.

## Acknowledgments

The authors thank Japan Petroleum Exploration Co., Ltd. and JGI, Inc. for permission to publish this paper.

## References

1. S.N. Madsen and H. N. Zebker, Imaging radar interferometry, In: *Principles and applications of imaging radar*, *vol. 2*, *Manual of remote sensing*, ed. F.M. Henderson, and A.J. Lewis, 3rd ed., New York; John Wiley & Sons, (1998) 359.
2. L.C. Smith, Emerging Applications of Interferometric Synthetic Aperture Radar (InSAR) in Geomorphology and Hydrology, *Annals, Assoc. Amer. Geogr.*, 92(3), (2002) 385.
3. D. Ebron, D. Buddery, G.Watts and B. Taylor, Monitoring activities at In Salah, paper presented at 2006 8th International Conference on Greenhouse Gas Control Technologies, Trondheim, Norway, June 19-22.
4. I.W. Wright, The In Salah Project: CO2 Storage Monitoring and Verification, paper presented at Carbon Sequestration Leadership Forum 2007 International Projects Workshop, Paris, Mar. 27.
5. F. Riddiford, I.W. Wright, C. Bishop, T. Espie and A. Tourqui, Monitoring geological storage The In Salah Gas CO2 Storage Project, paper presented at 2004 7th International Conference on Greenhouse Gas Control Technologies, Vancouver, Sept. 5-9.
6. R. Goldstein, Atmospheric limitations to repeat-track radar interferometry, *Geophys. Res. Lett.*, 22(18), (1995) 2,517.
7. D.T. Sandwell and E.J. Price, Phase gradient approach to stacking interferogram, *J. Geophys. Res.*, 103(B12), (1998) 30,183.
8. U. Wegmuller, C. Werner, T. Strozzi and A. Wiesmann, ERS-ASAR integration in the interferometric point target analysis, paper presented at Fringe 2005 Workshop, Frascati, Nov. 28 – Dec. 2.
9. P. Berardino, G. Fornaro, R. Lanari and E. Sansosti, A new algorithm for surface deformation monitoring based on small baseline differential SAR interferograms, *IEEE Trans. Geosci. Remote Sensing*, 40(11), (2002) 2,375.